The Journal of Immunology
RESEARCH ARTICLE | MARCH 15 2013

Increased Ribonuclease Expression Reduces Inflammation and Prolongs Survival in TLR7 Transgenic Mice FREE

Xizhang Sun; ... et. al

J Immunol (2013) 190 (6): 2536–2543.
https://doi.org/10.4049/jimmunol.1202689

Increased Ribonuclease Expression Reduces Inflammation and Prolongs Survival in TLR7 Transgenic Mice

Xizhang Sun,* Alice Wiedeman,† Nalini Agrawal,* Thomas H. Teal,* Lena Tanaka,* Kelly L. Hudkins,‡ Charles E. Alpers,‡ Silvia Bolland,§ Matthew B. Buechler,†,¶ Jessica A. Hamerman,†,¶ Jeffrey A. Ledbetter,* Denny Liggitt,‖ and Keith B. Elkon*,†

TLR7 activation is implicated in the pathogenesis of systemic lupus erythematosus. Mice that overexpress TLR7 develop a lupus-like disease with autoantibodies and glomerulonephritis and early death. To determine whether degradation of the TLR7 ligand RNA would alter the course of disease, we created RNase A transgenic (Tg) mice. We then crossed the RNase Tg to TLR7 Tg mice to create TLR7 × RNase double Tg (DTg) mice. DTg mice had a significantly increased survival associated with reduced activation of T and B lymphocytes and reduced kidney deposition of IgG and C3. We observed massive hepatic inflammation and cell death in TLR7 Tg mice. In contrast, hepatic inflammation and necrosis were strikingly reduced in DTg mice. These findings indicate that high concentrations of serum RNase protect against immune activation and inflammation associated with TLR7 stimulation and that RNase may be a useful therapeutic strategy in the prevention or treatment of inflammation in systemic lupus erythematosus and, possibly, liver diseases. ***The Journal of Immunology*****, 2013, 190: 2536–2543.**

Systemic lupus erythematosus is a potentially fatal disease caused by immune complexes deposition in the kidneys and other organs. Recently, it was discovered that, not only do immune complex cause tissue injury through activation of FcγR on myeloid cells and activation of the complement cascade (1), but they also enter plasmacytoid dendritic cells (pDC) to stimulate the production of type I IFN through activation of TLR (2). In mouse models of lupus, there is strong evidence to suggest that activation of TLR7, a receptor for ssRNA, plays a pivotal role in promoting lupus. This evidence includes marked attenuation of disease in MRL/Mp-*lpr*/*lpr* mice deficient in TLR7 (but not TLR9) (3), identification of an additional copy of TLR7 as being responsible for the accelerating effect of the Yaa mutation in BXSB mice (4, 5), and generation of a lupus-like disease in mice that have a knockin of TLR7 (6) (hereafter referred to as TLR7 transgenic [Tg] mice).

Because RNA is the ligand for TLR7 and because RNase treatment of apoptotic or necrotic extracts markedly reduces stimulation of type I IFN by pDC in vitro (reviewed in Ref. 7), we asked whether RNase would attenuate the expression of lupus in vivo. To this end, we created a mouse that constitutively secreted bovine RNase and crossed the RNase Tg to TLR7 knockin mice. Overexpression of RNase in TLR7 Tg mice resulted in a reduction in splenomegaly, reduced numbers of activated B and T cells, fewer immune deposits in the kidney, reduced liver inflammation, and increased survival.

Materials and Methods

Creation of bovine RNase Tg mice

Because the RNase gene contains no introns, bovine RNase was amplified from bovine genomic DNA by PCR using 5′-AATCCCGGGTCATCATGGCTCTGAAGTCC-3′ and 5′-GGACTAGTGGTAGAGACCTACACTGAAGCATCAA-3′ as primers. The amplified bovine RNase gene was cloned into PCRII-TOPO vector (Invitrogen Life Technologies, Carlsbad, CA) and then subcloned into Alb1L3NB-3 vector (provided by R. Palmiter, University of Washington, Seattle, WA) that uses the human albumin promoter resulting in hepatic expression of transgenes (8). Following sequence confirmation, the DNA fragment containing the albumin promoter and bovine RNase gene was transfected into the ES cells from C57BL/6 (B6) (75%) C3H (25%) mice, and selected ES cells were injected into blastocytes to generate Tg founders (called JLC mice). Founders were backcrossed to pure B6 mice for five generations to generate the RNase Tg line used in these studies. The same founder line for all studies reported. When comparing different genotypes, that is in crosses with other Tg mice, we used the same F_1 and littermate controls for the experiments.

Quantitation of RNase concentrations and activity by ELISA and single radial enzyme diffusion

RNase concentrations in serum were quantified by an in-house sandwich ELISA. In brief, ELISA plates were coated with a polyclonal anti-bovine RNase Ab (Abcam, Cambridge, MA) and detected with a biotinylated polyclonal anti-bovine RNase Ab (Rockland Immunochemicals, Gilbertsville, PA), followed by HRP–strepavidin (BioLegend, San Diego, CA) and substrate. Sera were tested at a 1/50 dilution. Bovine RNase (DNase free; Life Technologies) was used to create a standard curve. Functional RNase activity was quantified by single radial enzyme diffusion (SRED) (9) using poly-C (Sigma-Aldrich, St. Louis, MO) as a substrate. The gel was incubated for 4 h in a moist chamber at 37°C and then stained with ethidium bromide for 30 min on ice. The size of the rings was read under UV light and quantified using Carestream Molecular Imaging software (Kodak).

Serological analysis

Antinuclear Ab (ANA) were detected by indirect immunofluorescence using Hep-2 slides as a substrate at a dilution of 1/50. IgG anti-RNA Abs were detected by ELISA as previously described (10) using yeast RNA (10 μg/ml) (Sigma-Aldrich) as Ag. The purified mAb BWR4 (11, 12) was used to create a reference standard curve. Serum IgG anti-RNA subclasses were analyzed using the same ELISA but developed with subclass-specific

*Department of Medicine, University of Washington, Seattle, WA 98195; †Department of Immunology, University of Washington, Seattle, WA 98195; ‡Department of Pathology, University of Washington, Seattle, WA 98195; §Laboratory of Immunogenetics, National Institute of Allergic and Infectious Diseases, National Institutes of Health, Rockville, MD 20852; ¶Immunology Program, Benaroya Research Institute at Virginia Mason, Seattle, WA 98101; and ‖Department of Comparative Medicine, University of Washington, Seattle, WA 98195

Received for publication September 25, 2012. Accepted for publication January 7, 2013.

This work was supported by a grant from the Alliance for Lupus Research (to K.B.E.).

Address correspondence and reprint requests to Dr. Keith B. Elkon, Division of Rheumatology, University of Washington, Seattle, 1959 Northeast Pacific Street, Box 356428, Seattle, WA 98195. E-mail address: elkon@u.washington.edu

The online version of this article contains supplemental material.

Abbreviations used in this article: ANA, antinuclear Ab; B6, C57BL/6; DTg, double transgenic; LDG, low-density granulocyte; pDC, plasmacytoid dendritic cell; SLE, systemic lupus erythematosus; SRED, single radial enzyme diffusion; Tg, transgenic; WT, wild-type.

Abs (Sigma-Aldrich) as previously described (13), except that for all subclass analysis, anti-IgG2c rather than IgG2a was used as appropriate for the B6 background. For IgG2b, the mAb H564 (provided by T. Imanishi-Kari, Tufts University, Boston, MA) (14) was used to create a standard curve, but for other subclasses, selected TLR7 Tg serum (for IgG1 and IgG2c) or H564 serum (IgG3) with the highest OD value was used to create a standard curve. Total serum IgG in 4-mo-old mice was quantified by a sandwich ELISA as described previously (13). To detect anti-bovine RNase Abs, plates were coated with bovine RNase (5 μg/ml), and sera from 4-mo-old mice were tested at a dilution of 1/50.

Flow cytometry analysis and flow sorting

Spleen samples were pressed through a 40-μm cell strainer to generate a single-cell suspension that was depleted of RBCs by treatment with Ack lysing buffer. For flow-based sorting following sacrifice, splenocytes were incubated with 200 μg DNase (Sigma-Aldrich) and 8 mg type IV collagenase (Worthington Biochemical, Lakewood, NJ). After 25 min, cell dissociation buffer (Invitrogen) was added to 15% final volume for an additional 5 min. For surface staining, $\sim 2 \times 10^6$ cells were stained with one of the following Ab as indicated in the figures: allophycocyanin-conjugated anti-mouse TCRβ-chain Ab, anti-mouse CD69 PE (eBioscience, San Diego, CA), PE anti-mouse CD45RB Ab, PE anti-mouse CD44 Ab, PerCP/cy5.5 anti-mouse CD19 Ab, PE anti-mouse CD86 Ab, and Alexa Fluor 488 anti-mouse CD80 Ab. Myeloid cells were identified by Alexa Fluor 647 anti-mouse CD11c, FITC anti-mouse CD11b Ab. All Abs were from BioLegend, except where indicated. Samples were incubated at 4°C for 30 min. Data were acquired using a FACSCanto (BD Biosciences, San Diego, CA) and analyzed using FlowJo software (Tree Star, Ashland, OR). In all cases, doublets were excluded by gating before gating on live cells using forward light scatter and side scatter (of light). To evaluate cytokine responses to TLR agonists, splenocytes from WT and TLR7 Tg mice were stimulated with the TLR7 or TLR4 ligands gardiquimod (200–800 ng/ml) or LPS (6–10 ng/ml), respectively, and simultaneously treated with GolgiStop. After 2–3 h, cells were stained with mAb against CD11b, Ly6C, Ly6G, and TNF. Cells to ≥95% purity were sorted using either a FACSAria or FACSVantage (BD Biosciences).

RNA preparation and quantitative real-time PCR

Total RNA was isolated from sorted cells using the RNeasy mini kit with on-column DNAse treatment (Qiagen, Valencia, CA). First-strand cDNA was generated using 25 ng RNA with the high-capacity cDNA RT-kit using random primers (Applied Biosystems, Foster City, CA). Reactions in duplicate (20 μl) were run on an ABI StepOne Plus using the primers shown in Supplemental Table II, and a two-stage cycle of 95°C for 15 s and 60°C for 1 min was repeated for 40 cycles followed by a dissociation stage. Threshold cycle values were determined by setting a constant threshold at 0.2, and fold changes in gene expression were then calculated using the $2^{-\Delta\Delta CT}$ method or relative expression method. The standard curve showed similar amplification efficiencies for each gene, and template concentrations were within the linear dynamic range for each of primer set.

Pathology

Kidneys and livers were preserved in 10% formalin and embedded in paraffin and were also snap-frozen in liquid nitrogen and TissueTek OCT compound (Sakura Finetek, Torrance, CA) and stored at −70°C. Paraffin embedded sections were stained with H&E or with periodic acid–Schiff stain. Quantitation of glomerular tuft area, macrophage infiltration using the Ab Mac-2, and immunfluorescence staining with goat anti-mouse IgG, IgG subclasses (Santa Cruz Biotechnology, Santa Cruz, CA), and C3 (Cappel, Westchester, PA) were performed as described previously (13).

A semiquantitative score of H&E-stained liver sections was given by a pathologist blinded to sample identity. This included a count of inflammatory foci (>20 cells/focus) per five random ×10 fields and a relative lesion severity score (range, 0–5) based on size, distribution, and presence of bridging between foci, presence of bile duct hyperplasia, and hepatocellular necrosis. Cleaved caspase-3 and the macrophage Ag F4/80 were detected by polyclonal rabbit anti-mouse (Biocare Medical, Concord, CA) and monoclonal rat anti-mouse (Life Technologies) Abs, respectively. Immunohistochemical procedures were performed on a Leica Bond–automated immunostainer using HRP-conjugated secondary Abs. Numbers of caspase-3–positive cells per millimeter of liver section area were expressed as positive cells per millimeter. Digital images were captured using a Nikon Digital Sight camera system with Nikon Instruments Elements software. Color and contrast of entire images were standardized using Nikon Instruments Elements software. No selective corrections were performed.

Statistical analysis

Statistical significance between groups was determined by ANOVA with Tukey's multiple comparison test, Mann–Whitney *U* test, or a Wilcoxon signed-rank test. A p value <0.05 was considered significant. Differences in proportions were calculated by the χ^2 test. Graphs and statistical analyses were performed using Prism software (Graphpad Software) or SigmaStat (Systat Software).

Results

Creation of single and double Tg mice that overexpress RNase

TLR7.1 Tg mice express TLR7 mRNA at 8- to 16-fold higher than WT control and develop a lupus-like disease characterized by immune activation, splenomegaly, and glomerulonephritis associated with the production of anti-RNA autoantibodies (6). Because it is presumed that ssRNA is the ligand that drives TLR7 activation in these mice, we developed a strategy to degrade extracellular RNA in TLR7 Tg mice. First, we generated wild-type (WT) mice on the B6 background that overexpressed bovine RNase A under control of the albumin promoter such that RNase A was secreted from the liver. These mice were born in normal Mendelian ratios and were healthy and fertile. Bovine RNase was detected in the serum at concentrations of ∼25 ng/ml in Tg mice, and SRED analysis revealed potent functional activity (Fig. 1A, 1B). On the basis of these results, the sp. act. of RNase in the serum of double Tg (DTg) mice was calculated as 0.05 U/μg. Because this is lower than the commercial bovine RNase standard (1 U/μg), this may be explained by optimization of the recombinant enzyme or serum factors that attenuate RNase activity.

Examination of spleen size and lymphocyte proportions and activation revealed no differences compared with non-Tg WT mice (Supplemental Fig. 1). The RNase Tg mice were crossed with TLR7.1 Tg mice to yield RNase × TLR7 DTg mice. Introduction of the RNase Tg to the TLR7 Tg mice also appeared to have no detrimental effects on litter size, and DTg mice were born in the expected ratios. DTg mice had serum RNase concentrations and activity similar to the RNase Tg mice (Fig. 1B, 1C). On the basis of SRED functional analysis, RNase activity in the DTg mice was estimated at ∼5-fold WT B6 mice (Fig. 1B, *lower panel*). The normal growth, maturation, fertility, and numbers of immune cells in RNase Tg mice indicate that the overexpression of RNase in the RNase Tg mice had no apparent adverse effects. No IgG Abs to bovine RNase were detected in TLR7 Tg or DTg mice (n = 10 in each group; data not shown).

Overexpression of RNase partially restores immune expansion and attenuates B and T cell activation

When we evaluated immune activation in RNase × TLR7 DTg mice at 3.5–4.0 mo of age, we observed that spleen weight was significantly reduced in DTg as compared with TLR7 Tg mice (Fig. 2A). Consistent with the reduction in spleen weight, the striking increase in the numbers of myeloid cells in TLR7 Tg mice (23-fold higher compared with B6 mice) was reduced to 12-fold in DTg mice, whereas the numbers of T and B cells were very similar between the two strains (Fig. 2B). The reduction in the numbers of myeloid cells in DTg mice resulted in partial restoration of the normal proportions of T and B cells in the spleen (Fig. 2C). Despite the increase in the proportions of B and T cells in DTg mice, the percentages of B and T cells that were activated were significantly reduced as determined by the expression of CD69 and CD80 (B cells) and CD69 and CD44 (T cells) (Fig. 2D).

Because we observed that B cell activation was reduced in DTg mice, we next looked for serologic differences between TLR7 Tg and DTg mice. There were no differences between the two strains in total serum IgG concentrations (median ± SD values

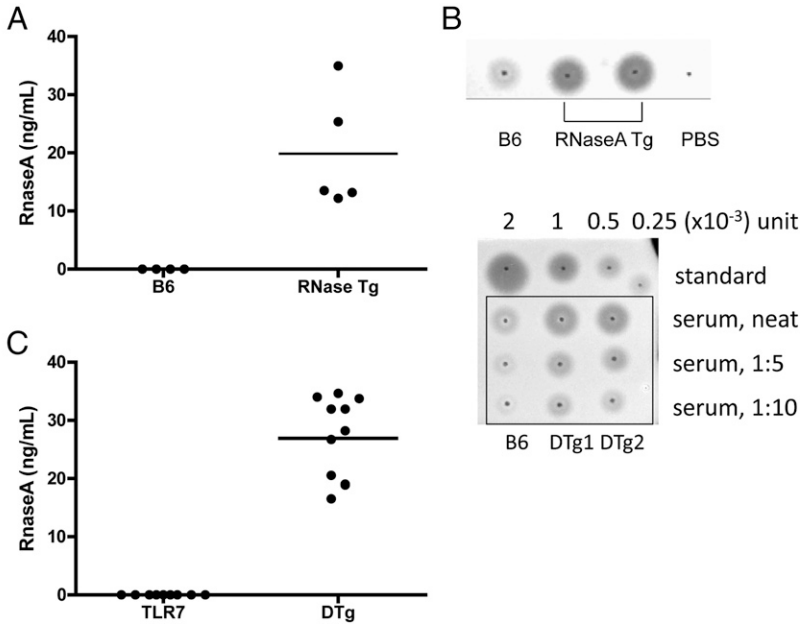

FIGURE 1. Expression of RNase in RNase Tg and DTg (RNase × TLR7, DTg) mice. (**A** and **C**) The concentration of transgene encoded bovine RNase in mouse serum was quantified by a sandwich ELISA (not cross-reactive with mouse RNase) using commercial bovine RNase to create a standard curve. (**B**) RNase functional activity was quantified by SRED as described in *Materials and Methods*. *Upper panel*, Serum from a normal WT B6 and two RNase Tg mice were tested. *Lower panel*, One B6 and two randomly selected DTg mice were tested neat and at the dilutions shown. In the top row, commercial RNase was used as a positive control and expressed as functional activity (units where 1 U is equivalent to 0.118 Kunitz Unit). Mice were 14–16 wk of age.

of 3161 ± 2084 and 3143 ± 2045 in TLR7 and DTg mice, respectively, $n = 10$/group; p = NS). TLR7 Tg mice develop anti-RNA Abs that produce cytoplasmic and nucleolar staining by immunofluorescence (6). We asked whether expression of RNase affected the levels of anti-RNA autoantibodies in a second large cohort of DTg mice for the survival study. As shown in Fig. 3A, there was no significant difference in anti-RNA autoantibody concentration in DTg mice compared with littermate controls. When younger (2-mo-old) mice were evaluated or the differences between percentage positive in the two strains were evaluated, no statistically significant differences were observed (data not shown). Consistent with these observations, no obvious reduction in intensity or alteration in the pattern of immunofluorescence ANA staining were detected in the DTg mice (data not shown). We next evaluated the relative levels of IgG anti-RNA subclass Abs in older TLR7 and DTg mice. First, in TLR7 Tg mice, we observed that the concentrations of total IgG anti-RNA (Fig. 3A) and IgG2b anti-RNA were similar, whereas the other subclasses showed either no (IgG3) or only modest (IgG1 and IgG2c) elevations compared with B6 mice (Fig. 3B). When we compared subclass levels between TLR7 and DTg mice, there was a modest but statistically significant increase in IgG1 anti-RNA in DTg compared with TLR7 Tg mice but no other statistical differences in subclass distribution (Fig. 3B). We have previously used the ratio between IgG1 and 2a(c) as an indirect measure of CD4 Th cell skewing and nephrogenicity (13, 15). As shown in Fig. 3B, there was a significant reduction in the IgG2c/IgG1 ratio in DTg com-

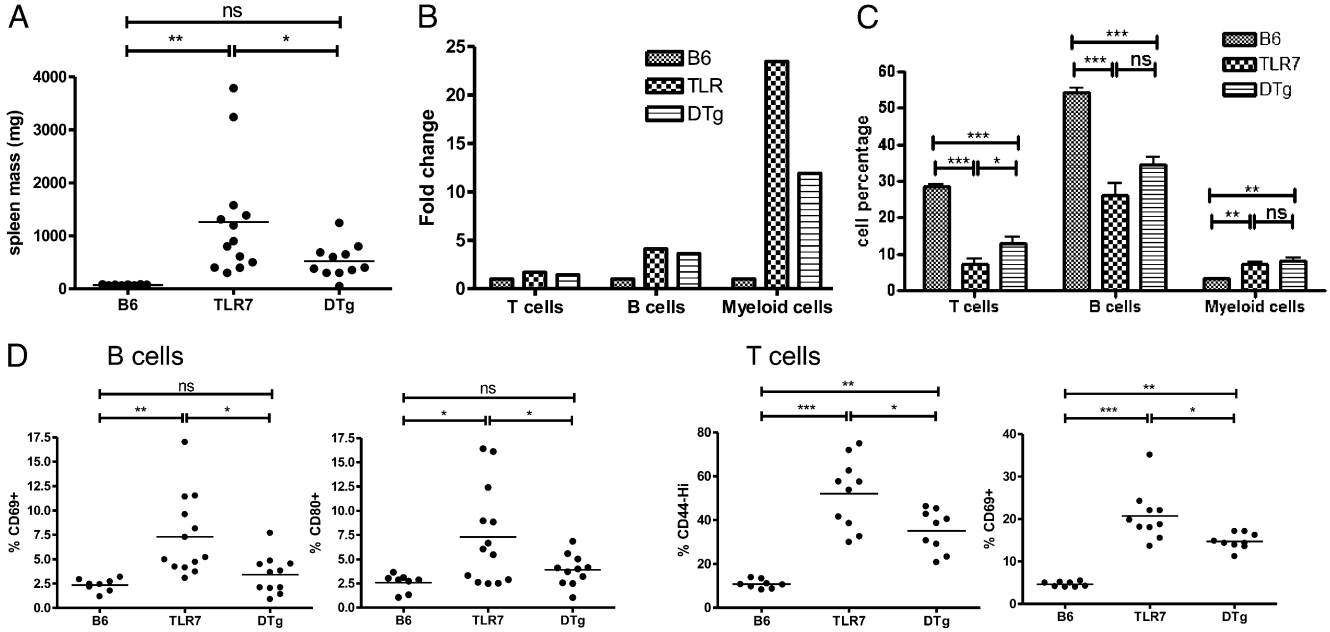

FIGURE 2. DTg mice have a reduction in spleen size, myeloid expansion, and T and B cell activation. Mice were sacrificed ~3.5 mo of age, and the spleen weight was determined (**A**). (**B**) Flow cytometry of splenocytes was performed using the phenotypic markers TCR-β (T cells), CD19 (B cells), and CD11b (myeloid cells), and the fold increase of T, B, and myeloid cells was calculated as a ratio of the number of cells in TLR7 or DTg mice/the number of cells in WT B6 control mice. In (**C**), the relative percentage of T, B, and myeloid cells was determined by flow cytometry analysis. In (**D**) the percentage of B and T cells that expressed the activation markers CD69 and CD80 (B cells) or CD69 and CD44 (T cells) are shown. $*p < 0.05$, $**p < 0.01$, $***p < 0.001$.

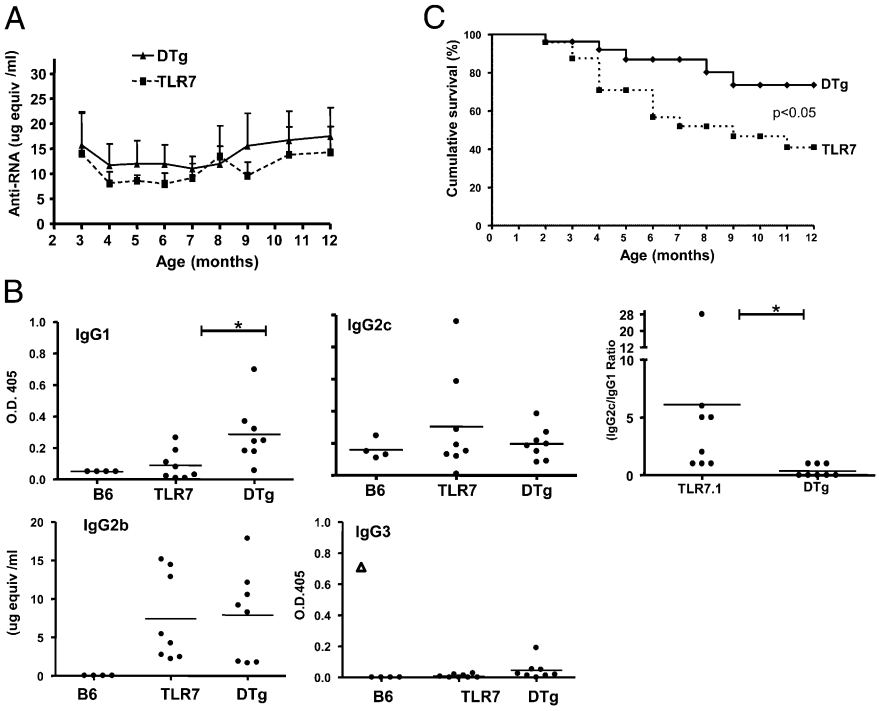

FIGURE 3. IgG anti-RNA autoantibodies persist in DTg mice but show alterations in subclass distributions and DTg mice have a significant improvement in survival. TLR7 and DTg mice (n = 25 and 19 mice, respectively) were bled monthly. Total IgG (**A**) and IgG subclass [(**B**), at 10–12 mo of age] anti-RNA Abs were quantified by ELISA as described in *Materials and Methods*. Anti-RNA mAb were used to construct standard curves for total IgG and IgG2b anti-RNA, and the results were expressed as microgram equivalents. For IgG1, IgG2c, and IgG3, no anti-RNA mAb were available so results are expressed as OD. Because IgG3 anti-RNA was uniformly low in TLR7 mice, a serum from H564 mouse was used as a positive control (△). Differences in anti-RNA Ab levels between TLR7 and DTg were not statistically significant, except where indicated. (**C**) The same mice as in (A) were followed for survival, and the Kaplan–Meier survival curve was plotted over a 12-mo period. Significance was determined by the log-rank test using GraphPad Prizm software. *$p <$ 0.05.

pared with TLR7 Tg mice. Taken together, these findings suggest an alteration in Th skewing affecting subclass distribution in DTg mice, but the Th1-associated subclass IgG2b (16) remained the dominant anti-RNA subclass in both TLR7 Tg and DTg mice.

RNase overexpression leads to improvement in survival and reduced immune deposits in the kidneys in TLR7 Tg mice

Because we had observed improvement in some, but not all, measures of immune function in DTg mice, we compared survival between DTg and TLR7.1 littermate controls in a second large cohort of mice. As shown in Fig. 3C, there was a highly significant difference in survival of DTg mice compared with littermate controls. At 7 mo, 50% of TLR7.1 littermate controls had died, whereas only 13% of DTg were dead. This finding indicates that, despite the lack of effect on anti-RNA Ab titers in this strain, overexpression of RNase exerted a strong therapeutic effect.

The reasons why TLR7.1 mice die prematurely is not entirely clear although severe anemia, thrombocytopenia, and glomerulonephritis could play a part (6). To determine whether red cell and platelet counts were positively impacted by RNase therapy, we performed blood counts but found no significant differences between in the two strains (results not shown). With regard to renal function, <10% of mice had >1+ proteinuria over the time of observation, and there were no significant differences in proteinuria between DTg and TLR7 Tg mice (data not shown).

Histologic sections from kidney tissue at 14–16 wk stained with the periodic acid–Schiff reagent showed mild expansion of mesangial regions that was qualitatively similar between TLR7 and DTg mice. Glomeruli were without prominent inflammatory cell infiltration, sclerosis, hypercellularity, or histologic evidence of prominent immune complex deposition such as intracapillary accumulations of "hyaline thrombi" or subendothelial capillary wall deposits of the type seen in severe proliferative lupus nephritis. Although no statistically significant differences in IgG and C3 deposition were observed by indirect immunofluorescence in DTg mice at 3.5 mo, we observed significantly less IgG and C3 deposition in mice sacrificed at the termination of the survival study (Fig. 4). Semiquantitative analysis of immunofluorescence staining (scale 0–4) was total IgG: 2.8 ± 0.15 and 1.2 ± 0.15; C3 2.8 ± 0.14 and 1.6 ± 0.24 for TLR7 Tg and DTg, respectively ($p < 0.005$ for both IgG and C3; n = 7–9 mice/group). In view of alterations in the serum concentrations of anti-RNA subclass Abs in DTg mice, we examined subclass distribution of IgG in their kidneys by Abs validated in a previous study (13). IgG1 and IgG3 staining was similar to the B6 control staining (data not shown). However, IgG2b and IgG2c were consistently detected in TLR7 Tg mice but significantly reduced in intensity in the DTg mice (Fig. 4). Semiquantitative analysis was IgGb: 2.2 ± 0.13 and 0.8 ± 0.06; IgG2c 2.3 ± 0.26 and 0.8 ± 0.14 for TLR7 Tg and DTg, respectively (n = 4–7 mice/group; $p < 0.005$ for both). In summary, TLR7.1 DTg mice survived longer than their single Tg counterparts and had a reduction in total IgG and C3 deposition in their kidneys associated with reduced deposits of the complement fixing isotypes IgG2b and IgGc at a late time point in their disease.

RNase overexpression rescues TLR7 Tg mice from severe hepatic inflammation

Recently, Fukui et al. (17) engineered a mutation, D34A, that leads to a selective loss of TLR9 binding but enhanced TLR7 binding to Unc93B1, resulting in markedly enhanced TLR7 signaling. The most striking pathology in the D34A mutant was observed in the liver where severe inflammation and patchy necrosis were observed (17). Some inflammation in the liver, but not the lung, was previously noted in TLR7 Tg mice (6). Because the hepatic inflammation and necrosis was considered the most likely cause of death in Unc93B D34A mutant mice and we also detected elevated liver transaminases in TLR7 Tg moribund mice as did Fukui et al. (17), we compared the liver pathology in TLR7 single Tg and DTg mice.

Hepatic lesions in TLR7 Tg mice aged 12–14 wk were distinct and typically characterized by large, dense, and frequently confluent accumulations of primarily mononuclear inflammatory cells within portal and periportal locations but also, on occasion, surrounding central veins (Fig. 5, Supplemental Table I). In portal regions, inflammatory cell accumulation was accompanied by disruption of the limiting plate and replacement of adjacent hepatic parenchymal cells by dense F4/80 Ag–positive accumulations of tissue macro-

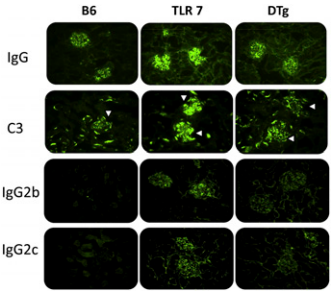

FIGURE 4. Representative frozen sections from kidneys obtained from mice aged 12 mo (n = 4–9 mice/group) were stained by indirect immunofluorescence for IgG, IgG subclasses, and C3. Glomerular staining for C3 is delineated by white arrowheads. Semiquantitative assessment of staining intensity is reported in *Results*. IgG1 and IgG3 staining was minimal and not different among B6, TLR7, and DTg mice (data not shown). Original magnification ×40.

phages intermixed with lymphocytes, some fibroblasts, and neutrophils (Fig. 5B, 5E, 5K, 5L). Hemosiderin-laden macrophages and pooled erythrocytes were also common in many inflammatory foci suggesting chronic microvascular disruption. In some areas, adjacent portal triads were bridged or partially bridged by this chronic/active inflammatory process. Bile duct hyperplasia was common within severely affected portal regions (Fig. 5E) of these mice. Hepatocellular apoptosis and necrosis typically involved individual cells within the region of the limiting plate and at the margin of larger inflammatory foci (Fig. 5E, 5G). In contrast, DTg mice had substantially less severe lesions as evidenced by the presence of a lower lesion severity score and fewer inflammatory cell foci compared with TLR7 Tg mice (Fig. 5C, 5F, 5M, Supplemental Table I). The lessened severity of the lesions was due to smaller, more widely scattered inflammatory cell accumulations and mild-to-nonexistent bile duct hyperplasia or bridging of portal regions. Scattered foci of extramedullary hematopoiesis were present within livers of both TLR 7.1 and DTg mice, whereas cell death was much more prominent in TLR7 Tg mice as determined by staining with Ab to activated caspase-3 (Fig. 5H–J). TLR7 Tg and DTg mice had 3.45 ± 1 versus 0.85 ± 0.51 caspase-3–positive cells per square millimeter, respectively; p = 0.04).

Inflammatory monocytes produce TNF in response to TLR7 stimulation

Because myeloid cells were prominent in the liver infiltrates as determined by positive staining with F4/80 (Fig. 5L), we first addressed whether TLR7 expression was increased in peripheral myeloid cells. We found that flow-sorted splenic inflammatory monocytes ($CD11b^{high}Ly6C^{high}Ly6G^{negative}$) and neutrophils ($CD11b^{high}Ly6G^{high}Ly6C^{high}$) obtained from TLR7 Tg mice expressed 5- to 10-fold more TLR7 mRNA compared with WT B6 mice, equivalent to TLR7 expression levels in pDC (18) or B cells (6) in this strain. Of considerable interest, the splenic neutrophils, but even more so the inflammatory monocytes defined by surface markers described in *Materials and Methods*, expressed much higher levels of genes encoding granule proteins associated with neutrophils: myeloperoxidase, cathepsin G, proteinase 3, and elastase compared with WT (Fig. 6A).

In view of the prominent myeloid expansion, liver infiltration, and high TLR7 expression in myeloid cells in TLR7 Tg mice, we asked whether myeloid cells from TLR7 Tg mice responded abnormally to TLR7 agonists. We focused on TNF rather than IFN-α because TLR7 Tg mice show only modest increases in IFN response genes (see Fig. 5 in Ref. 6), and TNF rather than type I IFN is strongly associated with liver inflammation and hepatocyte

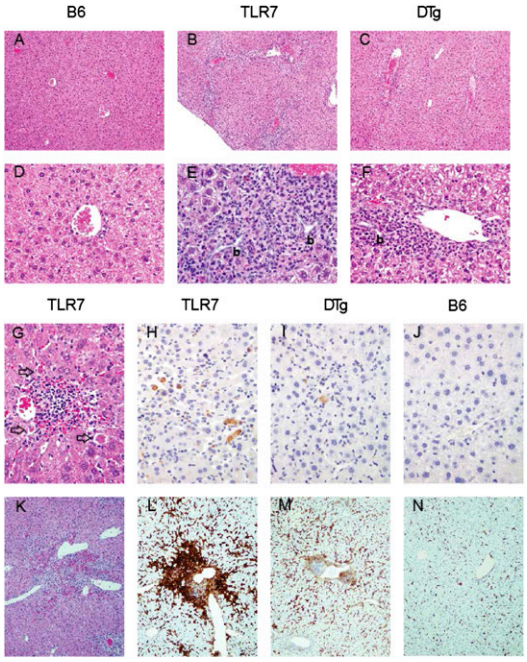

FIGURE 5. DTg mice have a marked reduction in hepatic inflammation and necrosis relative to TLR7 Tg mice. Representative liver sections from control (B6), TLR7.1, and DTg mice. Sections of WT liver [(**A**), ×10; (**D**), ×40) showing normal hepatic structure. A normal portal triad is centrally placed in plate D. Liver from TLR7 Tg mice demonstrates bridging between triads by highly cellular inflammatory and stromal elements [(**B**), ×10]. At ×40 (**E**), portal triads are fully surrounded by tissue macrophages (some of which contain brown hemosiderin pigment) admixed with lymphocytes, neutrophils, and fibrous tissue elements. Bile duct hyperplasia (b), limiting plate necrosis, and apoptosis of individual hepatocytes occur in severely affected triads (E). DTg mice have a similar type of inflammatory hepatitis, although much less severe and rarely bridges adjacent triads [(**C**), ×10; (**F**), ×40]. Similarly, bile duct hyperplasia (b), limiting plate necrosis, and apoptosis are less common and milder in degree. The lower severity of hepatic inflammation in DTg mice is reflected by a lower lesion severity score of 2.1 ± 1.1 (compared with 4.3 ± 0.8 for TLR7 Tg, n = 6/group; p = 0.006) and fewer inflammatory cell foci (8.2 ± 5.8 per random ×10 field compared with 32.6 ± 5.8 for TLR7 Tg mice; p = 0.001). See *Materials and Methods* for definitions and Supplemental Table I for analysis of individual mice. Classical shrunken apoptotic hepatocytes (arrows) are common typically near margins of inflammatory foci [(**G**), ×40] and revealed by staining with Ab to activated caspase-3 [light brown in (**H**)–(**J**), ×40]. F4/80 staining of the inflammatory foci in TLR7.1 mice [(B), ×10; (E), ×40; (**K**), ×10] revealed intense staining surrounding triads and central veins [dark brown, (**L**), ×10].

death as demonstrated in many other situations (19, 20). Inflammatory monocytes, but not neutrophils, from bone marrow and spleen obtained from TLR7 Tg mice responded with significantly higher levels of TNF compared with WT cells following stimulation with gardiquimod (TLR7 agonist) but not LPS (TLR4 agonist) (Fig. 6B). Similar findings were observed with inflammatory monocytes obtain from DTg mice (data not shown). No difference in IL-6 expression was observed (data not shown). Significantly, TNF mRNA expression was elevated in the livers of TLR7 Tg mice but significantly reduced in DTg mice (Fig. 6C). Taken together, these findings implicate TNF in liver injury and show reduced expression of this cytokine in DTg mice.

Discussion

We observed that when the lupus-prone mouse strain TLR7 Tg overexpressed RNase, it was partially protected from inflammation in the kidney and, more strikingly, in the liver and had a significant

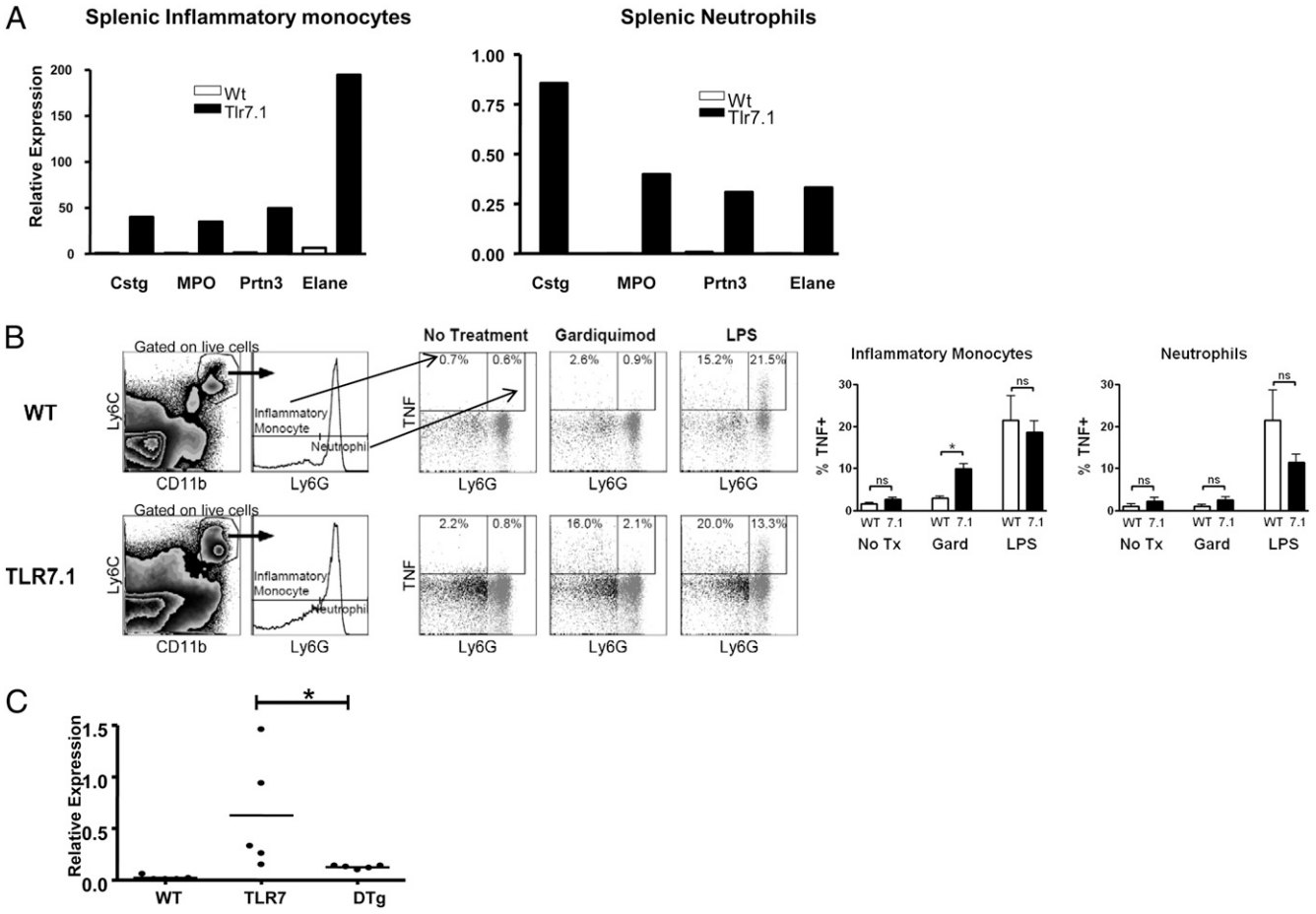

FIGURE 6. Myeloid cells from TLR7 Tg mice express high levels of proteases and produce TNF on activation. (**A**) Splenic neutrophils and inflammatory monocytes were purified by flow cytometry, RNA isolated and quantitative PCR for the genes shown performed on mice aged 3 mo as described in *Materials and Methods*. Results are expressed relative to the ribosomal 18S RNA control. (**B**) Total spleen cells from WT and TLR7 Tg mice were stimulated with the TLR7 or TLR4 ligands, gardiquimod (800 ng/ml), or LPS (10 ng/ml), respectively. After 3 h, cells were stained with mAb against CD11b, Ly6C, Ly6G, and TNF. Inflammatory monocytes ($CD11b^{high}Ly6C^{high}Ly6G^{negative}$) and neutrophils ($CD11b^{high}Ly6G^{high}Ly6C^{high}$) were identified (*left panel*) and the intracellular expression of TNF in the populations examined by flow cytometry. A representative result is shown in the *middle panel* (where the percentage positive refers to TNF positive in that cell type) and the average of three experiments in the *right panel*. (**C**) Quantitative PCR for TNF was compared in 10-wk-old WT, TLR7 Tg, and DTg mice. $*p < 0.05$.

improvement in survival. Overexpression of RNase itself had no obvious adverse effects as determined by clinical manifestations or early mortality in RNase Tg mice. Furthermore, detailed evaluation of immune cellular composition in this strain appeared to be normal. Although variant forms of RNase such as frog (*Rana pipiens*) RNase (Onconase) have been used as a chemotherapeutic drug in certain types of cancer (21), RNase A, which is normally present in the circulation, is not cytotoxic (22). This is explained by differences in the binding of Onconase and RNase A to the cell surface membrane as well as the fact that RNase A, but not Onconase, is bound by the cytosolic RNase inhibitor with femtomolar affinity and efficiently neutralized (23).

Unc93B1is an endoplasmic reticulum resident protein that controls TLR3, 7, and 9 transport as evidenced by the loss of function of these TLRs in '3d' mice with the H412R missense mutation (24). In contrast, the D34A mutation results in a loss of ligand binding to TLR9 but increased activation of TLR7 (17). The striking similarity between the phenotype of mice with the Unc93B1 D34A mutation and the TLR7 Tg mice used in the current study, including myeloid expansion, anemia, thrombocytopenia, and mild glomerulonephritis, indicates that it is the enhanced response to TLR7 ligand rather than overexpression of TLR7 that causes disease in these genetically altered strains of mice.

Similar to findings in the Unc93B1 D34A mice (17), we observed severe inflammation and patchy necrosis in the livers of TLR7 Tg mice, which was likely the major contributor to death. In the DTg mice, however, hepatic inflammation was markedly attenuated, and fewer dying cells were detected. Whether local overexpression of RNase by hepatocytes is necessary for the beneficial effects of the enzyme in the liver will need to be tested in the future by alternative modes of RNase delivery.

What accounts for the severe hepatic injury in TLR7 Tg mice? Behrens et al. (25) recently showed that repetitive TLR9 stimulation causes macrophage activation and hepatitis and that this syndrome was predominately caused by innate immune system activation. Because myeloid cells were prominent in the liver infiltrates, these cells are likely major contributors to liver injury. Significantly, we observed that both inflammatory monocytes and neutrophils isolated in the periphery expressed 5- to 10-fold more TLR7 mRNA compared with WT B6 mice, indicating that they may be more sensitive to TLR7 ligands. Indeed, inflammatory monocytes from TLR7 Tg mice produced significantly higher levels of TNF following stimulation with a TLR7 ligand. Although TNF alone may not be sufficient to kill hepatocytes, it primes Kupffer cells and neutrophils to release cytotoxic mediators (26, 27) and is strongly implicated in hepatic injury in is-

chemia reperfusion injury (28). Consistent with the reduction in inflammation in the livers of DTg mice, TNF mRNA expression was significantly reduced in the livers of DTg mice, implying that a reduction in the physiologic ligand for TLR7, RNA, led to both reduced expansion and activation of myeloid cells in the livers of DTg mice.

Precisely how innate immune cells are activated in the liver of TLR7 Tg mice remains to be determined. Dying hepatocytes as a potential source of RNA were readily demonstrated in the livers of TLR7 Tg mice, so they likely perpetuate TLR7 activation. Neutrophils that were readily identifiable by their characteristic morphology release both DNA and RNA, which, when bound to cathelicidin (LL37), are potent stimulators of TLR9 and TLR7, respectively (29). Finally, apoptotic CD8 T cells that also die in the liver (30) may contribute to the load of dying cells in the liver and stimulate cytokine production in cells that are hyperresponsive to TLR7.

Of considerable interest, both the inflammatory monocytes as well as the neutrophils from TLR7 Tg mice expressed much higher levels of mRNA encoding granulocyte proteases compared with WT control mice. This signature is reminiscent of immature monocytes emerging from the bone marrow (http://www.immgen.org) and likely reflects abnormal myelopoiesis (18). Of clinical relevance, PBMC from SLE patients express a granulocyte signature, which is explained by the presence of a low-density granulocyte (LDG) fraction that comprises a mixed population of early granulocyte/monocyte precursors (myelocytes) (31, 32). These LDG produce inflammatory cytokines, including TNF, and are implicated in vascular cytotoxicity in SLE (32). Thus, the inflammatory monocyte population described in this study bears many similarities to the LDG subpopulation in SLE.

A surprising finding in this study was that there was no statistically significant change in anti-RNA Ab activity over time in DTg mice. This finding may be because anti-RNA autoantibodies in TLR7.1 mice are only very modestly elevated (6) and varied considerably between mice. Low and variable levels of anti-RNA autoantibodies are also consistent with our findings that kidney damage was very mild in the TLR7 Tg mice. Although glomerulonephritis was previously thought to be an important contributor to death in TLR7 Tg mice, we observed that very few of these mice had evidence of severe nephritis on histology or impaired function as determined by proteinuria. Nevertheless, the reduction in immune deposits at late time points in DTg mice without a change in the total circulating anti-RNA autoantibodies titers suggested that either a different Ab specificity deposits in the glomeruli, that the circulating RNase may partially degrade the immune complex, rendering it less efficient at tissue deposition and complement fixation, and/or that there was a change in anti-RNA isotype.

A recent study by S. Bolland and coworkers (33) determined that B cell activation in TLR7 Tg mice has a B cell–intrinsic component but can also be driven by T cells. Transcript expression studies of TLR7 Tg follicular B cells revealed increased expression of IgG2b but not IgG2a(c) (33). Consistent with this observation, we found that most serum anti-RNA Abs belong to the IgG2b subclass. When we compared subclass distribution of anti-RNA Abs between TLR7 and DTg mice, we observed an increase in the IgG1 subclass and reduction in the IgG2c/IgG1 ratio of anti-RNA in the DTg mice, suggesting a change in the Th1 to Th2 cell autoantibody drive. Coupled with the reduced B and T cell activation observed in DTg mice, these findings are consistent with partial degradation of Ag by RNase leading to alteration in TLR7 stimulation and possibly the affinity/avidity of AgRs impacting B cell maturation (34) and/or Th cell skewing (35, 36). We have, in fact, observed changes in B cell maturation in the spleens of DTg mice (N.V. Giltiay, C.P. Chappell, X. Sun, N. Kolhatkar, T.H. Teal, A. Wiedeman, J. Kim, M.B. Buechler, J.A. Hamerman, E.A. Clark, and K.B. Elkon, submitted for publication). No significant alteration in the levels of IgG2b, 2c, or 3 anti-RNA Abs between TLR7 and DTg mice were seen. Because both IgG2c and IgG2b are considered to be driven by Th1 cells (16), yet the IgG2b subclass remained elevated in DTg mice, it suggests that other cytokines such as TGF-β and/or IL-6 may play a role in stimulating this autoantibody (37). Whereas IL-6 and TGF-β promote differentiation of Th17 cells, IL-17 deficiency did not reduce autoantibody production in TLR7 Tg mice (33). Future studies will be needed to address which APC (macrophage, dendritic cell, and B cell), what cytokines and T cell subsets drive anti-RNA, and how Ag degradation by RNase impacts each of these components of the autoimmune response.

When we examined the subclasses deposited in the kidneys in older mice, we observed that there was very little deposition of IgG1 and 3 in either the TLR7 or DTg strains but that there was a significant reduction in IgG2b and IgG2c deposition in DTg mice. Whereas a decrease in IgG2c staining can be explained by reduced serum levels in some mice (Fig. 3), the reduced renal deposition of IgG2b without a change in serum levels is most consistent with the idea that RNase partially degrades the immune complex, rendering it less efficient at tissue deposition. Because both IgG2b and c are complement activating subclasses (16), their reduction in glomerular deposits explains the total reduction of IgG and C3 fixation in the kidney.

In conclusion, overexpression of RNase exerts a strong protective effect in a TLR7-driven mouse model with lupus-like features and liver inflammation and death. DTg mice had a reduction in spleen size, reduced myeloid cell expansion, and reduced activation of B and T cells compared with TLR7 Tg mice. These observations provide evidence that prior to activation of endosomal TLR7, the RNA ligand is accessible to extracellular RNase. Precisely where RNA is released to impact lymphocyte function is uncertain, although ongoing studies suggest that one site is the spleen and influences B cell maturation (N.V. Giltiay et al., submitted for publication). These findings raise the possibility that treatment of established lupus-like or inflammatory liver disease with therapeutics to degrade RNA will be an effective strategy for treatment of SLE and other disorders where inflammation is driven by RNA that not only activates TLR7 but also TLR3, TLR8, and the retinoic acid–inducible gene I family (retinoic acid–inducible gene-like receptors) (38).

Acknowledgments

We thank Nick Crispe (Seattle Biomedical Research Institute, Seattle, WA) for review of the manuscript and Martha Hayden Ledbetter (University of Washington) for helpful comments.

Disclosures

K.B.E., J.A.L., and X.S. have commercial interest in Resolve Therapeutics. In addition, K.B.E. and J.A.L. are cofounders of the company Resolve Therapeutics. K.B.E., J.A.L., and X.S. hold intellectual property to a patent for RNase use in SLE. The other authors have no financial conflicts of interest.

References

1. Rahman, A., and D. A. Isenberg. 2008. Systemic lupus erythematosus. *N. Engl. J. Med.* 358: 929–939.
2. Lövgren, T., M. L. Eloranta, B. Kastner, M. Wahren-Herlenius, G. V. Alm, and L. Rönnblom. 2006. Induction of interferon-α by immune complexes or liposomes containing systemic lupus erythematosus autoantigen- and Sjögren's syndrome autoantigen-associated RNA. *Arthritis Rheum.* 54: 1917–1927.
3. Christensen, S. R., J. Shupe, K. Nickerson, M. Kashgarian, R. A. Flavell, and M. J. Shlomchik. 2006. Toll-like receptor 7 and TLR9 dictate autoantibody

specificity and have opposing inflammatory and regulatory roles in a murine model of lupus. *Immunity* 25: 417–428.
4. Pisitkun, P., J. A. Deane, M. J. Difilippantonio, T. Tarasenko, A. B. Satterthwaite, and S. Bolland. 2006. Autoreactive B cell responses to RNA-related antigens due to TLR7 gene duplication. *Science* 312: 1669–1672.
5. Subramanian, S., K. Tus, Q. Z. Li, A. Wang, X. H. Tian, J. Zhou, C. Liang, G. Bartov, L. D. McDaniel, X. J. Zhou, et al. 2006. A Tlr7 translocation accelerates systemic autoimmunity in murine lupus. *Proc. Natl. Acad. Sci. USA* 103: 9970–9975.
6. Deane, J. A., P. Pisitkun, R. S. Barrett, L. Feigenbaum, T. Town, J. M. Ward, R. A. Flavell, and S. Bolland. 2007. Control of Toll-like receptor 7 expression is essential to restrict autoimmunity and dendritic cell proliferation. *Immunity* 27: 801–810.
7. Martin, D. A., and K. B. Elkon. 2005. Autoantibodies make a U-turn: the Toll hypothesis for autoantibody specificity. *J. Exp. Med.* 202: 1465–1469.
8. Pinkert, C. A., D. M. Ornitz, R. L. Brinster, and R. D. Palmiter. 1987. An albumin enhancer located 10 kb upstream functions along with its promoter to direct efficient, liver-specific expression in transgenic mice. *Genes Dev.* 1: 268–276.
9. Yasuda, T., D. Nadano, K. Sawazaki, and K. Kishi. 1992. Genetic polymorphism of human deoxyribonuclease II (DNase II): low activity levels in urine and leukocytes are due to an autosomal recessive allele. *Ann. Hum. Genet.* 56: 1–10.
10. Blanco, F., J. Kalsi, and D. A. Isenberg. 1991. Analysis of antibodies to RNA in patients with systemic lupus erythematosus and other autoimmune rheumatic diseases. *Clin. Exp. Immunol.* 86: 66–70.
11. Eilat, D., and R. Fischel. 1991. Recurrent utilization of genetic elements in V regions of antinucleic acid antibodies from autoimmune mice. *J. Immunol.* 147: 361–368.
12. Lau, C. M., C. Broughton, A. S. Tabor, S. Akira, R. A. Flavell, M. J. Mamula, S. R. Christensen, M. J. Shlomchik, G. A. Viglianti, I. R. Rifkin and A. Marshak-Rothstein. 2005. RNA-associated autoantigens activate B cells by combined B cell antigen receptor/Toll-like receptor 7 engagement. *J. Exp. Med.* 202: 1171–1177.
13. Hughes, G. C., D. Martin, K. Zhang, K. L. Hudkins, C. E. Alpers, E. A. Clark, and K. B. Elkon. 2009. Decrease in glomerulonephritis and Th1-associated autoantibody production after progesterone treatment in NZB/NZW mice. *Arthritis Rheum.* 60: 1775–1784.
14. Berland, R., L. Fernandez, E. Kari, J. H. Han, I. Lomakin, S. Akira, H. H. Wortis, J. F. Kearney, A. A. Ucci, and T. Imanishi-Kari. 2006. Toll-like receptor 7-dependent loss of B cell tolerance in pathogenic autoantibody knockin mice. *Immunity* 25: 429–440.
15. Georgiev, M., L. M. Agle, J. L. Chu, K. B. Elkon, and D. Ashany. 2005. Mature dendritic cells readily break tolerance in normal mice but do not lead to disease expression. *Arthritis Rheum.* 52: 225–238.
16. Nimmerjahn, F., and J. V. Ravetch. 2010. Antibody-mediated modulation of immune responses. *Immunol. Rev.* 236: 265–275.
17. Fukui, R., S. Saitoh, A. Kanno, M. Onji, T. Shibata, A. Ito, M. Onji, M. Matsumoto, S. Akira, N. Yoshida, and K. Miyake. 2011. Unc93B1 restricts systemic lethal inflammation by orchestrating Toll-like receptor 7 and 9 trafficking. *Immunity* 35: 69–81.
18. Buechler, M., T. H. Teal, K. Elkon, and J. Hamerman. Cutting edge: type I IFN drives emergency myelopoiesis and peripheral myeloid expansion during chronic TLR7 signaling. *J. Immunol.* In press.
19. Leist, M., F. Gantner, I. Bohlinger, P. G. Germann, G. Tiegs, and A. Wendel. 1994. Murine hepatocyte apoptosis induced in vitro and in vivo by TNF-α requires transcriptional arrest. *J. Immunol.* 153: 1778–1788.
20. Yi, A. K., H. Yoon, J. E. Park, B. S. Kim, H. J. Kim, and A. Martinez-Hernandez. 2006. CpG DNA-mediated induction of acute liver injury in D-galactosamine-sensitized mice: the mitochondrial apoptotic pathway-dependent death of hepatocytes. *J. Biol. Chem.* 281: 15001–15012.
21. Fang, E. F., and T. B. Ng. 2011. Ribonucleases of different origins with a wide spectrum of medicinal applications. *Biochim. Biophys. Acta* 1815: 65–74.
22. Leich, F., N. Stöhr, A. Rietz, R. Ulbrich-Hofmann, and U. Arnold. 2007. Endocytotic internalization as a crucial factor for the cytotoxicity of ribonucleases. *J. Biol. Chem.* 282: 27640–27646.
23. Haigis, M. C., E. L. Kurten, and R. T. Raines. 2003. Ribonuclease inhibitor as an intracellular sentry. *Nucleic Acids Res.* 31: 1024–1032.
24. Tabeta, K., K. Hoebe, E. M. Janssen, X. Du, P. Georgel, K. Crozat, S. Mudd, N. Mann, S. Sovath, J. Goode, et al. 2006. The Unc93b1 mutation 3d disrupts exogenous antigen presentation and signaling via Toll-like receptors 3, 7 and 9. *Nat. Immunol.* 7: 156–164.
25. Behrens, E. M., S. W. Canna, K. Slade, S. Rao, P. A. Kreiger, M. Paessler, T. Kambayashi, and G. A. Koretzky. 2011. Repeated TLR9 stimulation results in macrophage activation syndrome-like disease in mice. *J. Clin. Invest.* 121: 2264–2277.
26. Bautista, A. P., A. Schuler, Z. Spolarics, and J. J. Spitzer. 1991. Tumor necrosis factor-α stimulates superoxide anion generation by perfused rat liver and Kupffer cells. *Am. J. Physiol.* 261: G891–G895.
27. Nathan, C., S. Srimal, C. Farber, E. Sanchez, L. Kabbash, A. Asch, J. Gailit, and S. D. Wright. 1989. Cytokine-induced respiratory burst of human neutrophils: dependence on extracellular matrix proteins and CD11/CD18 integrins. *J. Cell Biol.* 109: 1341–1349.
28. Colletti, L. M., D. G. Remick, G. D. Burtch, S. L. Kunkel, R. M. Strieter, and D. A. Campbell, Jr. 1990. Role of tumor necrosis factor-α in the pathophysiologic alterations after hepatic ischemia/reperfusion injury in the rat. *J. Clin. Invest.* 85: 1936–1943.
29. Guiducci, C., C. Tripodo, M. Gong, S. Sangaletti, M. P. Colombo R. L. Coffman, and F. J. Barrat. 2010. Autoimmune skin inflammation is dependent on plasmacytoid dendritic cell activation by nucleic acids via TLR7 and TLR9. *J. Exp. Med.* 207: 2931–2942.
30. Huang, L., G. Soldevila, M. Leeker, R. Flavell, and I. N. Crispe. 1994. The liver eliminates T cells undergoing antigen-triggered apoptosis in vivo. *Immunity* 1: 741–749.
31. Bennett, L., A. K. Palucka, E. Arce, V. Cantrell, J. Borvak, J. Banchereau, and V. Pascual. 2003. Interferon and granulopoiesis signatures in systemic lupus erythematosus blood. *J. Exp. Med.* 197: 711–723.
32. Denny, M. F., S. Yalavarthi, W. Zhao, S. G. Thacker, M. Anderson, A. R. Sandy, W. J. McCune, and M. J. Kaplan. 2010. A distinct subset of proinflammatory neutrophils isolated from patients with systemic lupus erythematosus induces vascular damage and synthesizes type I IFNs. *J. Immunol.* 184: 3284–3297.
33. Walsh, E. R., P. Pisitkun, E. Voynova, J. A. Deane, B. L. Scott, R. R. Caspi, and S. Bolland. 2012. Dual signaling by innate and adaptive immune receptors is required for TLR7-induced B-cell-mediated autoimmunity. *Proc. Natl. Acad. Sci. USA* 109: 16276–16281.
34. Pillai, S., and A. Cariappa. 2009. The follicular versus marginal zone B lymphocyte cell fate decision. *Nat. Rev. Immunol.* 9: 767–777.
35. Tao, X., C. Grant, S. Constant, and K. Bottomly. 1997. Induction of IL-4-producing $CD4^+$ T cells by antigenic peptides altered for TCR binding. *J. Immunol.* 158: 4237–4244.
36. Blander, J. M., D. B. Sant'Angelo, K. Bottomly, and C. A. Janeway, Jr. 2000. Alteration at a single amino acid residue in the T cell receptor α chain complementarity determining region 2 changes the differentiation of naive CD4 T cells in response to antigen from T helper cell type 1 (Th1) to Th2. *J. Exp. Med.* 191: 2065–2074.
37. McIntyre, T. M., D. R. Klinman, P. Rothman, M. Lugo, J. R. Dasch, J. J. Mond, and C. M. Snapper. 1993. Transforming growth factor β1 selectivity stimulates immunoglobulin G2b secretion by lipopolysaccharide-activated murine B cells. *J. Exp. Med.* 177: 1031–1037.
38. Takeuchi, O., and S. Akira. 2010. Pattern recognition receptors and inflammation. *Cell* 140: 805–820.